

energy of 3.245 GeV and beam currents of 20–25 μA incident upon specially developed high density cryogenic targets for $A = 1\text{--}4$. The helium target lengths were approximately 4 cm, the thicknesses being 310 mg/cm² (³He) and 546 mg/cm² (⁴He), $\pm 1\%$ respectively. The backgrounds from uncorrelated (e' , K^+) pairs, as well as contributions from the aluminum walls of the cryogenic targets, were subtracted in the charge normalized yields.

The scattered electrons were detected in the high momentum spectrometer (HMS, momentum acceptance $\Delta p/p \approx \pm 10\%$, solid angle ~ 6.7 msr) in coincidence with the electroproduced kaons, detected in the short orbit spectrometer (SOS, momentum acceptance $\Delta p/p \approx \pm 20\%$, solid angle ~ 7.5 msr). The detector packages of the two spectrometers are very similar [3]. Two drift chambers near the focal plane, utilized for reconstructing the particle trajectories, are followed by two pairs of segmented plastic scintillators that provide the main trigger signal as well as time-of-flight information. The time-of-flight resolution is ~ 150 ps(σ). For electron identification, a lead-glass shower detector array is used together with a gas threshold Čerenkov, in order to distinguish between e^- and π^- . For kaon identification in the SOS, a silica aerogel detector ($n = 1.034$) provided K^+/π^+ discrimination while an acrylic Čerenkov counter ($n = 1.49$) was used for K^+/p discrimination. Utilizing time-of-flight together with the Čerenkov detectors, kaons are clearly separated from background pions and protons [4,5]. Electroproduction processes exchange virtual photons, γ^* , between projectile and target. The spectrometer angle for electron detection was kept fixed during the experiment, thereby holding the virtual photon flux constant (cf. Ref. [6]). The angle of the kaon arm was varied to measure angular distributions with respect to

the direction of γ^* . The invariant mass of γ^* was $Q^2 = 0.35$ GeV², the total energy in the photon-nucleon system was $W = 1.91$ GeV. The ${}^3,4\text{He}(e, e'K^+)X$ process was studied for three different angle settings between γ^* and the ejected kaon (K), $\theta_{\gamma^*K^+}^{\text{lab}} \approx 1.7^\circ, 6^\circ, 12^\circ$, that correspond to increasing the momentum transfer to the hypernucleus [$|t| \approx (0.12, 0.14, 0.23)$ GeV²]. The central spectrometer momenta were 1.29 GeV/ c for the kaon arm and 1.58 GeV/ c for the electron arm.

The final states, X , in ${}^3,4\text{He}(e, e'K)X$ in the reconstructed missing mass spectra of the recoiling system are shown in Fig. 1, were identified using the four-momenta q of the virtual photon, p_K of the outgoing kaon, and total missing momentum P_{miss} , $M_x^2 = (q + P_{\text{miss}} - p_K)^2$. For ⁴He, a ⁴ Λ H bound state is clearly visible for all three angles just below the ³H- Λ threshold of 3.925 MeV. For ³He, just below the ²H- Λ threshold of 2.993 MeV, the ³ Λ H bound state is barely visible as a weak shoulder for 1.7 $^\circ$, but clearly present for 6 $^\circ$ and 12 $^\circ$.

Two states of the ⁴ Λ H system are known [1], the ground state with a binding energy of (2.04 ± 0.04) MeV, $J^\pi = 0^+$, and an excited state, bound by (1.00 ± 0.06) MeV, $J^\pi = 1^+$. The experimental resolution of ~ 4 MeV is, however, not sufficient to resolve the ground and excited states of the ⁴ Λ H system. The calibration of the missing mass spectrum has been performed using elastic ¹H($e, e'p$) data as well as ¹H($e, e'K^+)\Lambda$ data, both obtained during the same experiment. The precision of the calibration is estimated to be better than 1 MeV. Since the missing mass spectra have not been shifted with respect to the known binding energy of the ⁴ Λ H state after calibration, the observed agreement shows the adequacy of the procedure. Inasmuch as electroproduction has a large spin-flip probability in the forward direction [7], the excited state of the ⁴ Λ H system should be favored and the

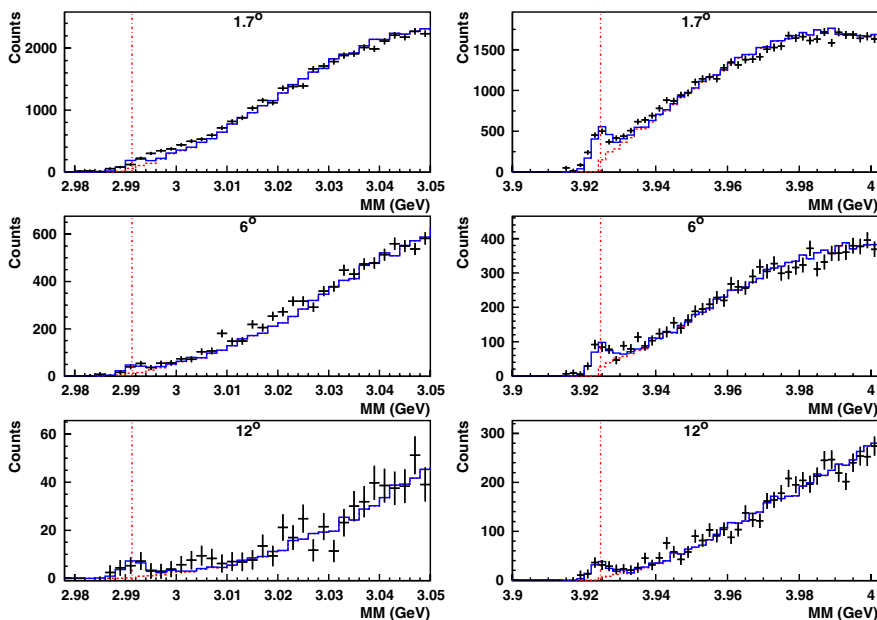


FIG. 1 (color online). Reconstructed missing mass spectra for ³He (left) and ⁴He (right) targets in the region of quasifree Λ production for different kinematic settings. Data points are shown with statistical error bars. Simulations of the quasifree (QF) reactions ${}^3,4\text{He}(e, e'K^+)$ are shown by dashed lines. Solid lines represent the sum of simulations of the QF background and the bound state reactions, ${}^3,4\text{He}(e, e'K^+){}^3,4\Lambda\text{H}$. The thresholds for QF production, $\Lambda + {}^2\text{H}$, $\Lambda + {}^3\text{H}$, respectively, are denoted by vertical lines.

data interpreted as a superposition of the ground and excited states, where the excited state is favored even more strongly closer to 0° .

The electroproduction cross section may be written as

$$\frac{d^5\sigma}{d\Omega_e dE_e d\Omega_K} = \Gamma \frac{d\sigma}{d\Omega_K},$$

where $(d\sigma/d\Omega_K)$ is the virtual photon cross section and Γ denotes the virtual photon flux factor, viz

$$\Gamma = \frac{\alpha}{2\pi} \frac{E'_e}{E_e} \frac{1}{Q^2} \frac{1}{1-\epsilon} \frac{W^2 - M^2}{2M},$$

where M is taken to be the nucleon mass. The experimental cross sections were extracted using a Monte Carlo simulation that modeled the optical conditions of the spectrometers, kaon decays, small angle scattering, energy losses and radiative corrections [5,8]. The ${}^3\text{He}(e, e'K^+)_{\Lambda}{}^3\text{H}$ bound state production process was modeled assuming coherent production off a stationary target nucleus. In order to facilitate the subtraction of the unresolved quasifree tail underneath the bound state region, the quasifree ${}^3\text{He}(e, e'K^+)X$ processes off nucleons inside the target nuclei, ${}^3\text{He}$ had to be modeled as well [9]. Since no models are available for the electroproduction on $A = 3, 4$ nuclei, we use an elementary cross section model [5,10] which is convolved by spectral functions [11] for ${}^3\text{He}$. Our dedicated model was shown to describe our ${}^1\text{H}(e, e'K^+)_{\Lambda}$ data best over the acceptance [10]. Final state interactions in the vicinity of the respective quasifree thresholds were taken into account by using an effective range approximation [12] which gave satisfactory results as shown in Fig. 1.

The uncertainty of fitting the strength of the background to the quasifree continuum is the dominant source of the error of the cross section for the bound state distributions, particularly for the low yields for the ${}^3_{\Lambda}\text{H}$ bound states, this results in large uncertainties. Furthermore, since the effective range approximation is very simple and takes into account only 2-body

Λ -nucleon interactions, a model dependent error has been estimated by fitting the shape of the quasifree tail with a simple parabolic function. This results in larger background subtractions and leads to cross sections $\sim 20\%$ lower than for the effective range ansatz. Thus the background was estimated to be the mean of the two results with an additional error derived from the differences of the two cases. Any other sources of systematic uncertainties are on a few per cent level. The extracted cross sections are given in Table I. For the angular distribution shown in Fig. 2, data were restricted to a common covered range in azimuthal angle of $(180 \pm 24)^\circ$ (last three rows of Table I). The point to point systematic uncertainties are $\sim 36\%$, 39% , 50% ; 11% , 16% , 23% ; 4.4% , 1.5% , 1.4% for ${}^3\text{He}$, ${}^4\text{He}$, ${}^1\text{H}$, respectively. For the setting with near parallel kinematics, 1.7° , however, the full azimuth was covered (first row of Table I). For these data, the point to point systematic uncertainties are $\sim 15\%$, 4.3% , 4.4% for ${}^3\text{He}$, ${}^4\text{He}$, ${}^1\text{H}$, respectively. For both ${}^3_{\Lambda}\text{H}$ and ${}^4_{\Lambda}\text{H}$ the cross section at 6° is a factor of 2 lower than at 1.7° . The 12° data point for ${}^3_{\Lambda}\text{H}$, however, strongly deviates from this behavior, making the ${}^3_{\Lambda}\text{H}$ angular distribution flatter than for ${}^4_{\Lambda}\text{H}$.

Figure 3 shows the ratio $R = \sigma_{\text{lab}}({}^3\text{He})/\sigma_{\text{lab}}({}^1\text{H})$ of the laboratory cross sections of ${}^3\text{He}(e, e'K^+)_{\Lambda}{}^3\text{H}$ to the cross section on the free proton. R is related to the nuclear form factor $F(k)$ by $R(k) = S \cdot W_A^2 \cdot F^2(k)$ [13], where k is the three momentum transfer to the hypernucleus, S is a spin factor, and W_A combines phase space and flux factors. We calculate $R(k)$ for our kinematics using $W_A = 2.1(1.68)$, $k = 2.02(2.08)$, $2.19(2.23)$, $2.69(2.69)$ fm^{-1} for ${}^3_{\Lambda}\text{H}$ (${}^4_{\Lambda}\text{H}$). For ${}^3_{\Lambda}\text{H}$ we take the parametrization of $F(k)$ and $S = 1/6$ of Ref. [13], in which Gaussian approximations for the underlying ${}^2\text{H}$, ${}^3\text{He}$ wave functions are used. For ${}^4_{\Lambda}\text{H}$ an expression of $F(k)$ similar to the ${}^3_{\Lambda}\text{H}$ case is derived [14], using Gaussian approximations for the underlying ${}^3\text{H}$, ${}^4\text{He}$ wave functions and the charge elastic form factors of ${}^3\text{He}$ of Ref. [15] for parametrization, and $S = 2$ for symmetry reasons. At 1.7° the calculated reduction of the elementary cross section by the form factor is ~ 250 (${}^3_{\Lambda}\text{H}$) and 100 (${}^4_{\Lambda}\text{H}$). The shape of the calculated $R(k)$ for

TABLE I. Differential cross sections for electroproduction of ${}^3_{\Lambda}\text{H}$ and ${}^4_{\Lambda}\text{H}$ bound states. In the laboratory, σ_{lab} denotes the fivefold differential cross section $d^5\sigma/d\Omega_e dE_e d\Omega_K$, σ_{cm} denotes the twofold differential cross section $d^2\sigma/d\Omega$ in the virtual photon-nucleus center of mass system. The last two columns give the cross section for the ${}^1\text{H}(e, e'K^+)_{\Lambda}$ process, obtained during the same experiment. The combined statistical and systematic errors are given. The first row shows data for 1.7° averaged over the azimuth. The θ_{cm} angles corresponding to θ_{lab} of 1.7° , 6° , 12° are 2.7° , 9.5° , 18.9° ; 2.5° , 8.7° , 17.4° ; 4.6° , 16.0° , 31.7° ; for ${}^3\text{He}$, ${}^4\text{He}$, and ${}^1\text{H}$ targets, respectively.

$\theta_{\gamma^* K^+}^{\text{lab}} (^\circ)$	${}^3_{\Lambda}\text{H}$		${}^4_{\Lambda}\text{H}$		Λ	
	$\sigma_{\text{lab}}(\text{nb}/\text{GeV}/\text{sr}^2)$	$\sigma_{\text{cm}}(\text{nb}/\text{sr})$	σ_{lab}	σ_{cm}	σ_{lab}	σ_{cm}
(1.7)	0.045 ± 0.008	5.15 ± 0.94	0.156 ± 0.008	20.83 ± 1.13	10.59 ± 0.21	465.01 ± 9.42
1.7	0.047 ± 0.020	5.27 ± 2.26	0.185 ± 0.025	24.70 ± 3.31	9.80 ± 0.52	430.43 ± 22.75
6	0.024 ± 0.011	2.77 ± 1.30	0.093 ± 0.018	12.36 ± 2.34	9.90 ± 0.17	437.31 ± 7.61
12	0.029 ± 0.017	3.38 ± 2.00	0.032 ± 0.009	4.47 ± 1.21	7.58 ± 0.13	363.78 ± 6.10

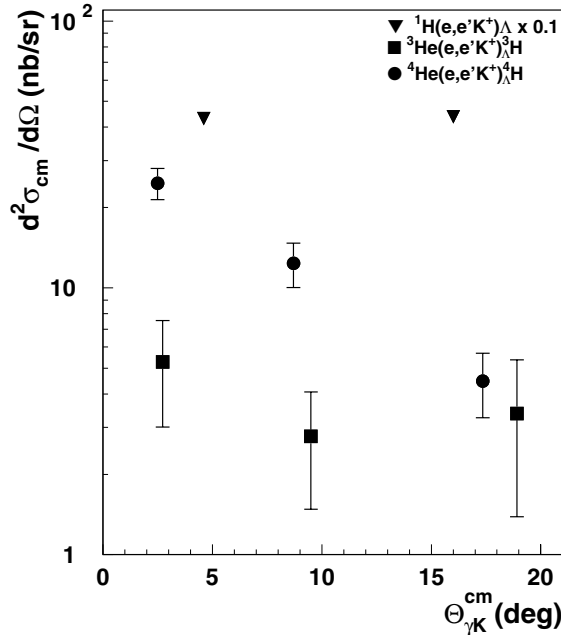


FIG. 2. Angular distributions of cross sections in the virtual photon-nucleus center of mass for the ${}^3\text{He}(e, e'K^+)_{\Lambda}{}^{3,4}\text{H}$ and ${}^1\text{H}(e, e'K^+)_{\Lambda}$ (scaled by 0.1) processes, plotted vs $\Theta_{\gamma K}^{\text{cm}}$. The data are given in Table I.

both hypernuclei is similar to the shape of the data for 1.7° and 6° , while it deviates for the 12° data. The latter may indicate a breakdown of approximating the underlying wave functions by Gaussians. For ${}^4_{\Lambda}\text{H}$ at 1.7° and 6° , the calculated $R(k)$ is 40%–50% higher than the data which suggests that the underlying wave functions are too simplistic such that their overlap is too large. Realistic wave functions obtained from Faddeev calculations are expected to give rise to more precise information. Future measurements at high three momentum transfer k would be highly desirable.

The production of the bound hypernuclei ${}^3_{\Lambda}\text{H}$ (hypertriton) and ${}^4_{\Lambda}\text{H}$ has been achieved for the first time in electroproduction and, for the first time in reaction spectroscopy, angular distributions for the ${}^3,4\text{He}(e, e'K^+)_{\Lambda}{}^{3,4}\text{H}$ processes have been obtained. The angular distribution for ${}^3\text{He}$ is flatter than for ${}^4\text{He}$ at large angles. Comparing these cross sections to the cross section on the free proton shows that the angular dependence of the cross section is determined by the nuclear form factor for small angles but deviates for larger angles. This should be tested by performing more precise calculations using realistic wave functions. These data and future measurements using dedicated spectrometer systems with resolutions below 1 MeV [16] may trigger a renaissance of the spectroscopy of the lightest hypernuclei that have not been studied since the first emulsion experiments many years ago.

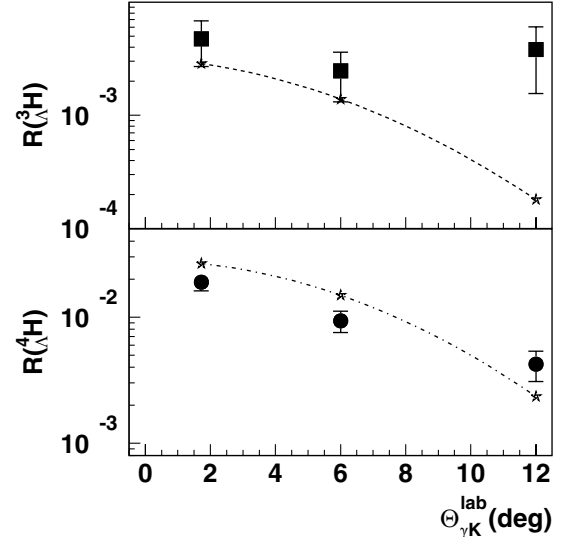


FIG. 3. Ratios $R = \sigma_{\text{lab}}({}^{3,4}\text{He})/\sigma_{\text{lab}}({}^1\text{H})$ for ${}^3_{\Lambda}\text{H}$ (upper panel) and ${}^4_{\Lambda}\text{H}$ (lower panel). The dashed and dot-dashed curves are related to the respective nuclear form factors calculated in Refs. [13,14].

We are grateful to H.W. Barz for calculating the He form factors and thank T. Mart for valuable communications. This work was supported in part by the DOE under Contract No. W-31-109-Eng-38 (ANL), Contract No. DE-AC05-84ER40150 (TJNAF), and the NSF. The excellent support of the staff of the Accelerator and Physics Division of TJNAF is gratefully acknowledged. F.D. acknowledges the support by the A.v.Humboldt-Stiftung, and the support by ANL for hosting this research.

*Electronic address: F.Dohrmann@fz-rossendorf.de

- [1] B. F. Gibson and E. V. Hungerford, *Phys. Rep.* **257**, 349 (1995).
- [2] M. Danyasz, *Nuovo Cimento Suppl.* **4**, 609 (1956).
- [3] G. Niculescu *et al.*, *Phys. Rev. Lett.* **81**, 1805 (1998).
- [4] D. Abbott *et al.*, *Nucl. Phys.* **A639**, 197 (1998).
- [5] R. M. Mohring *et al.*, *Phys. Rev. C* **67**, 055205 (2003).
- [6] B. Zeidman *et al.*, *Nucl. Phys.* **A691**, 37 (2001).
- [7] S. R. Cotanch and S. S. Hsiao, *Nucl. Phys.* **A450**, 419c (1986).
- [8] R. Ent *et al.*, *Phys. Rev. C* **64**, 054610 (2001).
- [9] A. Uzzle, dissertation, Hampton University, 2002.
- [10] J. Reinhold *et al.*, *Nucl. Phys.* **A684**, 470 (2001).
- [11] O. Benhar, A. Fabrocini, S. Fantoni, and I. Sick, *Nucl. Phys.* **A579**, 493 (1994).
- [12] J. Gillespie, *Final State Interactions* (Holden-Day, San Francisco, 1964).
- [13] T. Mart, L. Tiator, D. Drechsel, and C. Bennhold, *Nucl. Phys.* **A640**, 235 (1998).
- [14] H.W. Barz (private communications).
- [15] R. B. Wiringa, *Phys. Rev. C* **43**, 1585 (1991).
- [16] Y. Fujii *et al.*, *Nucl. Phys.* **A721**, 1079 (2003).